Equilibrium Phase Behavior of Polybutadiene/Polyisoprene Films: Binodals and Spinodals

Ellen Reister[†]

II. Institut für Theoretische Physik, Universität Stuttgart, 70550 Stuttgart, Germany

Marcus Müller*

Department of Physics, University of Wisconsin-Madison, 1150 University Avenue, Madison, Wisconsin 53706-1390

Sanat K. Kumar[‡]

Department of Chemical Engineering, Rensselaer Polytechnic Institute, Troy, New York 12180

Received December 22, 2004; Revised Manuscript Received April 7, 2005

ABSTRACT: We employ self-consistent field theory to calculate binodals and spinodals of an asymmetric binary polymer blend in a thin film. The film surface and substrate of the film attract both the same component via short-range interactions. The ratios of chain lengths, segment lengths, and segment volumes are chosen to match with experimental parameters for a mixture of deuterated polybutadiene (dPB) and polyisoprene (PI). The form and strength of the surface potentials cannot be determined directly from the experiments. Therefore, we study the phase behavior as a function of surface interaction strength and film width. We find an interesting interplay between spinodal instability and prewetting behavior that leads to four possible spinodals: The two spinodals on the dPB-rich side mark the stability of thin and thick PI enrichment layers near the surfaces, the two on the PI-rich side are associated with the attraction of the two formed dPB/PI interfaces and bulk-like composition fluctuations in the PI-rich phase. The prewetting behavior also influences the binodals on the dPB-rich side. Upon increasing the film thickness, we observe that the binodals approach their bulk location while the spinodals remain different from the spinodals in the bulk because, even in very thick films, the unstable modes are associated with interface fluctuations rather than bulk composition fluctuations. We further study scattering qualitatively by analyzing the free energy required to excite certain density modes and discuss consequences for the interpretation of scattering experiments.

I. Introduction

Thin polymer films have been the subject of many studies not only because of their technological significance as protective or dielectric coatings but also because the influence of confinement on the phase behavior of polymer mixtures still poses a challenging question that is far from being fully understood.[1−5] While polymers share the general features of phase and wetting behavior with mixtures of small molecules, these spatially extended molecules offer some distinct advantages: (i) The strength of fluctuation effects can be reduced by increasing the chain length. This remains true both for bulk composition fluctuations as well as for interface fluctuations (capillary waves). (ii) The wetting transition[3,4] in polymer blends typically occurs at a much larger incompatibility than the phase separation in the bulk, hence, bulklike composition fluctuations and interface fluctuations pertinent to wetting phenomena are well separated.[6] (iii) Effects of evaporation are negligible because of the vanishingly low vapor pressure, and the thickness of enrichment layers at surfaces is set by the molecules' extension, which is large enough to facilitate experimental observation.

In this study, we perform self-consistent field (SCF)[7−11] calculations of an asymmetric polymer mixture confined between two symmetric hard walls. Because of the suppression of fluctuations in the mixture caused by the length of the polymer chains, SCF theory is very successful in describing polymer systems quantitatively well, and the binodals and spinodals of a system can be determined rather accurately. The binodals are the coexistence lines that express the values of the composition, the order parameter of the transition, in the two phase-separated, coexistent phases.

Spinodals can only be defined in a mean field theory. In the vicinity of the binodal, the homogeneous state is metastable, and phase separation is a thermally activated process that evolves through the formation of a nucleus of the thermodynamically stable phase. Further, inside the miscibility gap, the homogeneous state becomes absolutely unstable, and phase separation occurs spontaneously. The spinodal marks the border between thermally activated phase separation (nucleation) and spontaneous phase separation (spinodal decomposition). It is important to remark that the spinodal is a mean field concept. When one includes fluctuations into the considerations, there is no sharp distinction between the two modes of phase separation. If the thermal activation barrier of nucleation becomes comparable to the strength of thermal fluctuations, k_BT, a single nucleus can no longer be conceived as the well-defined transition state, and a gradual and broad crossover (spinodal nucleation) between the two modes of phase transition occurs.[12]

Polymer blends are the ideal experimental system to test these concepts because fluctuations are strongly

* Author to whom correspondence should be addressed. E-mail: mueller@physics.wisc.edu.
† E-mail: reister@theo2.physik.uni-stuttgart.de.
‡ E-mail: kumars5@rpi.edu.

10.1021/ma0473465 CCC: $30.25
Published on Web 05/18/2005

suppressed for long chains. Similar to the Ginzburg criterion that estimates the relevance of composition fluctuations in the vicinity of the critical point, there also exists a Ginzburg criterion for the relevance of fluctuations in the vicinity of the spinodal, ensuring that the region of spinodal nucleation decreases with increasing chain length.[12,13]

Recent experiments have raised open questions about the location of the spinodals in the bulk,[14] and there is even less known about the effect of confinement on the location of the spinodals. In the bulk, binodals and spinodals show a similar behavior, therefore, experimental analysis and certain theoretical methods often do not clearly distinguish between binodals and spinodals and neglect that they describe qualitatively different aspects of the phase behavior. Although this might lead to reasonable results in the bulk, the distinction between the two becomes essential for confined geometries. In the bulk, density fluctuations cause phase separation, in the thin film geometry interfacial fluctuations, that become unstable, are mainly responsible for phase separation. In thin polymer films it is, therefore, possible that the behavior of the binodal is similar to that of the bulk, but that the spinodal is significantly changed as will be shown in this paper.

Our analysis was motivated by experimental work[15] in which small-angle neutron scattering (SANS) measurements of two model polymer blends, deuterated polybutadiene/polyisoprene [dPB/PI] and deuterated polymethylbutylene/polyethylbutylene [dPMB/PEB], were performed to give insight into the change of phase behavior upon confinement. Both blends were regarded at bulk critical concentrations. In the bulk, the dPB/PI mixture phase separated upon increasing the temperature, while the dPMB/PEB blend showed the more common behavior of phase segregating upon reduction of temperature. Neutron reflectivity (NR) measurements that are sensitive to density profiles perpendicular to the film revealed that, in the thin film geometry, PI from the dPB/PI blend and dPMB from the dPMB/PEB blend were enriched close to both surfaces ("symmetric segregation"), i.e., the substrate and the air.[16−18] The inverse magnitude of concentration fluctuations, $1/I(q = 0)$, was studied as a function of inverse temperature, $1/T$. For the regarded thin films, the curves showed a minimum, which is an indication for the blends being off-critical in the thin film geometry. The measured inverse structure factor, $1/I(q = 0)$, was extrapolated to $1/I(q = 0) = 0$ to estimate the spinodal temperature, T_s, while the minimum was correlated with the location of the binodal. These estimates revealed for the dPD/PI films with widths smaller than 250 nm that the spinodal temperature, T_s, is shifted toward higher temperatures the thinner the film. The strong shift in the spinodal temperature in the experiments was one of the main motivations for studying the phase behavior of the system regarded in this work.

The interpretation of the experiments invoked strongly (irreversibly) adsorbed surface layers that give rise to nonequilibrium effects. Using SCF calculations, we cannot comment on these nonequilibrium effects but only consider full thermodynamic equilibrium. We calculate the location of the binodals and spinodals in the thin film geometry and compare our results with experiments. We can also investigate the ability of the experimentally performed extrapolation of the inverse structure factor in the one phase region to locate the spinodal.

To be able to compare experimental results of the dPB/PI mixture with our calculations, the parameters (chain length, segment length, segment volume, and Flory−Huggins parameter) are chosen to match with experimental findings. However, one of the problems in comparing experimental and theoretical results lies in identifying how the confining surfaces interact with the polymer film. Only general assumptions about the shape and strength of the surface fields can be made. To compare experimental results with theoretical calculations, it is, therefore, useful to analyze the phase behavior of a thin polymer blend as a function of the surface interaction, which is one of the main topics of this paper. The other question we address is scattering. Instead of calculating the exact scattering factor, we "simulate" scattering by exciting various density modes.

Our paper is organized in the following way. In the next section, we introduce the model underlying our SCF calculation and briefly introduce the numerical procedure. In Section 3, we explain how we map experimental parameters with those used in our calculations. In Section 4, we present binodals and spinodals for thin films of different widths and surface interaction strengths and explain how the observed different behavior of binodals and spinodals comes about. In the next section, we analyze the effects of scattering in a thin film. The paper finally closes with some conclusions.

II. Model

To get an understanding of experimental findings of the phase behavior in thin films of dPB/PI mixtures, we employ SCF calculations for binary polymer blends between two hard walls that equally attract one kind of monomer. Previous calculations of confined polymer mixtures[19−22] usually neglected the influence of the two polymer species not being symmetric. Experimental studies, however, reveal that the differences in segment size, chain length, etc., can be considerable. We, therefore, perform SCF calculations for polymer mixtures confined between two walls that take the asymmetry of the two species A and B into account explicitly.[23] The differences are expressed through the ratio of the chain lengths $\alpha = N_B/N_A$, of the statistical segment lengths $\beta = b_B/b_A$, and of the segmental volumes $\gamma = v_B/v_A$. ρ_A and ρ_B denote the volume fractions of the A and B segments, respectively, with the incompressibility constraint $\rho_A + \rho_B = 1$. All variables that are not explicitly noted by a subscript refer to the A component. We further define number fractions, $\phi_A = \rho_A/(\rho v_A) \equiv \rho_A$ and $\phi_B = \rho_B/(\rho v_B) = \rho_B/\gamma$. This leads to the incompressibility constraint $\phi_A + \gamma\phi_B = 1$. The interaction between A and B species may be expressed through the Flory−Huggins parameter, χ.

The walls confining the film are modeled as hard and impenetrable. In the boundary region, the total density drops from unity to zero. To capture this, the total density profile across the film is imposed and the incompressibility constraint takes the form, $\phi_A + \gamma\phi_B = \Phi_0$, with[6,24,25]

$$\Phi_0(x) = \begin{cases} \frac{1}{2}\left\{1 - \cos\left(\frac{\pi x}{\epsilon_w}\right)\right\} & \text{for } 0 \le x \le \epsilon_w \\ 1 & \text{for } \epsilon_w \le x \le D_0 - \epsilon_w \\ \frac{1}{2}\left\{1 - \cos\left(\frac{\pi(D_0 - x)}{\epsilon_w}\right)\right\} & \text{for } D_0 - \epsilon_w \le x \le D_0 \end{cases} \quad (1)$$

D_0 denotes the film thickness and ϵ_w is the width of the boundary region. The x-axis defines the axis perpendicular to the film throughout the whole paper. All length scales are measured in units of the end-to-end distance, $R_e = b_A\sqrt{N_A}$, of an A polymer. For all the results shown in this paper, we use $\epsilon_W = 0.15R_e$. This is rather large compared to the width of a liquid−vapor interface, but smaller values, ϵ_w, give rise to larger computational effort in the SCF calculations. Monomers interact via a short-range potential with the surfaces. Specifically, the surface interactions extend over the boundary region and are expressed through the field

$$h(x) = \begin{cases} \frac{4\Lambda R_e}{\epsilon_w}\left\{1 + \cos\left(\frac{\pi x}{\epsilon_w}\right)\right\} & \text{for } 0 \le x \le \epsilon_w \\ 0 & \text{for } \epsilon_w \le x \le D_0 - \epsilon_w \\ \frac{4\Lambda R_e}{\epsilon_w}\left\{1 + \cos\left(\frac{\pi(D_0 - x)}{\epsilon_w}\right)\right\} & \text{for } D_0 - \epsilon_w \le x \le D_0 \end{cases} \quad (2)$$

Positive values of Λ correspond to surfaces attracting the A component. The canonical partition function of our model takes the form

$$\mathcal{Z} \sim \frac{1}{n_A! n_B!} \int \mathcal{D}_A[\boldsymbol{r}]\mathcal{P}_A[\boldsymbol{r}] \int \mathcal{D}_B[\boldsymbol{r}]\mathcal{P}_B[\boldsymbol{r}] \times \exp(-\rho \int d^3\boldsymbol{r}\{\chi\hat{\phi}_A\hat{\phi}_B - h(\boldsymbol{r})(\hat{\phi}_A(\boldsymbol{r}) - \gamma\hat{\phi}_B(\boldsymbol{r}))\}) \times \delta(\Phi_0(\boldsymbol{r}) - \hat{\phi}_A(\boldsymbol{r}) - \gamma\hat{\phi}_B(\boldsymbol{r})) \quad (3)$$

where n_A and n_B denote the number of A and B polymers, respectively. The microscopic monomer densities $\hat{\phi}_A(\boldsymbol{r})$ and $\hat{\phi}_B(\boldsymbol{r})$ are given by

$$\hat{\phi}_A(\boldsymbol{r}) = N_A v_A \sum_{i=1}^{n_A} \int_0^1 d\tau\, \delta(\boldsymbol{r} - \boldsymbol{r}_i(\tau)) \quad (4)$$

$$\hat{\phi}_B(\boldsymbol{r}) = N_A \alpha v_A \sum_{i=1}^{n_B} \int_0^1 d\tau\, \delta(\boldsymbol{r} - \boldsymbol{r}_i(\tau)) \quad (5)$$

$\mathcal{P}_A[\boldsymbol{r}]$ and $\mathcal{P}_B[\boldsymbol{r}]$ denote the Gaussian distribution of the polymer chains, often referred to as the Wiener measure.[26] Performing a Hubbard−Stratonovich transformation that makes use of the relation

$$1 = \int \mathcal{D}\phi\delta(\phi - \hat{\phi}) \propto \int \mathcal{D}\phi\mathcal{D}W \exp\left[\frac{\rho}{N}\int_V d^3\boldsymbol{r} iW(\phi - \hat{\phi})\right] \quad (6)$$

the transformed partition function takes the form

$$\mathcal{Z} \sim \int \mathcal{D}\phi_A\mathcal{D}\phi_B\mathcal{D}W_A\mathcal{D}W_B\mathcal{D}\Xi \times \exp\{-F[\phi_A,\phi_B,W_A,W_B,\Xi]\} \quad (7)$$

with the new effective energy functional F

$$\frac{N}{\rho V}F[\phi_A,\phi_B,W_A,W_B,\Xi] = \frac{1}{V}\int_V d^3\boldsymbol{r}\{\chi N\phi_A(\boldsymbol{r})\phi_B(\boldsymbol{r}) - h(\boldsymbol{r})(\phi_A - \gamma\phi_B) - iW_A\phi_A - iW_B\phi_B + i\Xi(\phi_A + \gamma\phi_B - 1)\} - \bar{\phi}_A \ln Q_A[W_A] - \frac{\bar{\phi}_B}{\alpha}\ln Q_B[W_B] \quad (8)$$

Q_A and Q_B are the partition functions of a single polymer chain in an external field W_A and W_B, respectively. They are given by

$$Q_A = \int \mathcal{D}_A[\boldsymbol{r}]\mathcal{P}_A[\boldsymbol{r}] \exp[-\int_0^1 d\tau i W_A(\boldsymbol{r}(\tau))] \quad (9)$$

$$Q_B = \int \mathcal{D}_B[\boldsymbol{r}]\mathcal{P}_B[\boldsymbol{r}] \exp[-\alpha\int_0^1 d\tau i W_B(\boldsymbol{r}(\tau))] \quad (10)$$

SCF theory employs the mean field solution of this field theory by using the saddle point approximation for the integral in the partition function. This is equivalent to minimizing the effective energy functional, F, leading to the following set of equations that need to be solved self-consistently:

$$\frac{\delta F}{\delta i W_A} = 0: \quad \phi_A = -\bar{\phi}_A\frac{\delta Q_A}{\delta i W_A} \equiv \phi_A^* \quad (11)$$

$$\frac{\delta F}{\delta i W_B} = 0: \quad \phi_B = -\frac{\bar{\phi}_B}{\alpha}\frac{\delta Q_B}{\delta i W_B} \equiv \phi_B^* \quad (12)$$

$$\frac{\delta F}{\delta \phi_A} = 0: \quad -iW_A = \chi N\phi_B - H + i\Xi \quad (13)$$

$$\frac{\delta F}{\delta \phi_B} = 0: \quad -iW_B = \chi N\phi_A + \gamma H + \gamma i\Xi \quad (14)$$

ϕ_A^* and ϕ_B^*, that express the density of a single polymer chain in the external field iW_A and iW_B, respectively, may be calculated by introducing the propagators $q_A(\boldsymbol{r}, t)$ and $q_B(\boldsymbol{r}, t)$ that describe the probability to find the end of a chain of length t, with $0 \le t \le 1$, at position $\boldsymbol{r}$. For these propagators, the following diffusion-like equations hold:[8]

$$\frac{\partial q_A(\boldsymbol{r}, t)}{\partial t} = \frac{R_e^2}{6}\nabla^2 q_A(\boldsymbol{r}, t) - iW_A q_A(\boldsymbol{r}, t) \quad (15)$$

$$\frac{\partial q_B(\boldsymbol{r}, t)}{\partial t} = \frac{\alpha\beta^2 R_e^2}{6}\nabla^2 q_B(\boldsymbol{r}, t) - \alpha i W_B q_B(\boldsymbol{r}, t) \quad (16)$$

with the initial condition $q_A(\boldsymbol{r}, t = 0) = q_B(\boldsymbol{r}, t = 0) = 1$. Using the propagators that fulfill these equations, the single chain partition function is given by $Q_A = \int d^3\boldsymbol{r}\, q_A(\boldsymbol{r}, t = 1)$, and the densities are calculated by $\phi_A^* = (\bar{\phi}_A/Q_A)\int_0^1 dt\, q_A(\boldsymbol{r}, t)q_A(\boldsymbol{r}, 1 - t)$; for B, the equivalent relations apply.

In our SCF calculations that are performed only in one dimension, namely, perpendicular to the walls, all spatially varying variables are expressed as a Fourier expansion. The used basis functions are:

$$f_n(x) = \sqrt{2}\sin\left(\frac{n\pi x}{D_0}\right) \qquad n = 1, 3, 5,... \quad (17)$$

With the confining walls being symmetric, equilibrium density profiles have to be symmetric, i.e., only basis functions with odd indices are utilized. This expansion allows exact calculation of ϕ_A^* and ϕ_B^* for given fields

W_A and W_B. Equations 11−14 are numerically solved using the Newton−Broyden method.[27]

III. Choice of Parameters

As mentioned in the Introduction, this study is motivated by neutron reflectivity experiments of polymer blend films with one component (PI) strongly preferred at both the silicon substrate surface and the air surface.[17,18,15] At the critical composition, there are pronounced enrichment layers at the film surfaces separated by the dPB/PI interface from the dPB-rich center of the film. We choose our parameters to match those of the dPB/PI blend investigated in this study. The A species in our theory corresponds to dPB, and the B species to PI. The asymmetry of this blend is captured through the following ratios of the chain lengths and the statistical segment lengths:

$$\alpha \equiv \frac{N_B}{N_A} = 1.222, \quad \beta \equiv \frac{b_B}{b_A} = 1 \tag{18}$$

The ratio of the segment volumes, γ, and the relation between the Flory−Huggins parameter, χ, and temperature, T, are found by comparing the bulk behavior of the experiments with our model. The bulk Flory−Huggins free-energy density of the homogeneous system in our model is given by

$$f_{bulk} \equiv \frac{NF_{bulk}}{\rho V k_B T} = \phi \ln \frac{\phi}{e} + \frac{1-\phi}{\alpha\gamma} \ln \frac{1-\phi}{\alpha\gamma e} + \frac{\chi N}{\gamma}\phi(1-\phi) \tag{19}$$

This then yields the (exchange) chemical potential μ:

$$\mu_{bulk} \equiv \frac{df_{bulk}}{d\phi} = \ln \phi - \frac{1}{\alpha\gamma} \ln \frac{1-\phi}{\alpha\gamma} + \frac{\chi N}{\gamma}(1-2\phi) \tag{20}$$

The binodals and the coexistence value of the exchange chemical potential, μ_{coex}, are found through a double-tangent construction for the bulk free energy. The condition for the spinodal can be written in the form:

$$\frac{d\mu_{bulk}}{d\phi}\Big|_{spinodal} = \frac{1}{\phi} + \frac{1}{\alpha\gamma(1-\phi)} - \frac{2\chi N}{\gamma} \stackrel{!}{=} 0 \tag{21}$$

and with this, the critical point is located at:

$$\chi_c N = \frac{(1+\sqrt{\alpha\gamma})^2}{2\alpha} \quad \text{and} \quad \phi_c = \frac{1}{1+1/\sqrt{\alpha\gamma}} \tag{22}$$

Experimentally, the critical density of dPB in the regarded blend is $\phi_c = \rho_c(\text{dPB}) = 0.65$. Using $\alpha = 1.222$ leads to a ratio between the segment volumes of $\gamma = 2.82$. To convert the value of χN into a temperature, we use the formula

$$\chi = 7.526 \cdot 10^{-3} - \frac{1.809K}{T} \quad \text{or} \quad T[\text{K}] = \frac{3135}{13.043 - \chi N} \tag{23}$$

with $N = 1733$. This relation resembles the experimentally determined χ parameter, $\chi = 0.00541 - 1.4234K/T$ for a dPB/PI mixture.[17] The specific form is chosen to yield a critical temperature $T_c = 50$ °C. A possible composition dependence of the Flory−Huggins parameter is neglected. In any case, our qualitative findings do not depend on the precise relation between temperature (or composition) and the Flory−Huggins parameter.

To compare our results with experimental data, we finally need to find a mapping between the effective surface potential, that we introduce into our model, and the actual effect of the boundaries on the polymer mixture. This proves to be difficult because this information is not directly accessible from experimental results, so only estimated potentials can be used.

Before showing the influence of the surface potential strength and the film width on the phase diagrams, a few points regarding our modeling of the surfaces need to be elucidated: (i) Our model includes only short-range monomer−surface interactions; long-range, van der Waals interactions, which are present in experiments, are ignored. (ii) Because the density is reduced in the boundary zone, monomers in the vicinity of the surface suffer the "missing neighbor effect". Note that it is the width, ϵ_w, of the boundary region rather than the range of the monomer−monomer interactions (which vanishes) that determines the strength of the missing neighbor effect. Its strength might influence the order of the wetting transition. (iii) The form of the surface field is chosen such that its integrated strength is independent of the width, ϵ_w, of the boundary zone. In addition to this "enthalpic" surface field, there is a large entropic contribution to the surface free energy. The latter stems from packing of chains at the wall and (strongly) depends on the width, ϵ_w, of the boundary region. To a first approximation, the packing entropy is given by the Lifshitz formula:[28]

$$\Delta F \approx \frac{\rho b^2}{24} \int d^3\boldsymbol{r} \frac{|\nabla\phi(\boldsymbol{r})|^2}{\phi(\boldsymbol{r})} \sim \frac{\beta^2}{\gamma} \frac{R_e}{\epsilon_w} \frac{\rho R_e^3}{N} \frac{\text{area}}{R_e^2} \tag{24}$$

As the B component has a lower number density, $\gamma > 1$, it is enriched at the surface even for $\Lambda = 0$, and it takes a large positive "enthalpic" surface field $\Lambda N \sim R_e/\epsilon_w$ to compensate this entropic preference.

We emphasize that we do not expect our qualitative conclusions to be affected by the specific modeling of the surface properties because much of the following depends only on the shape of the effective interface potential that describes the interaction of the AB interface with the wall.[29] These qualitative features of the effective interface potential are determined by the location of the wetting transition and its order. For our model, the wetting transition is of first order in agreement with all experimentally observed wetting transitions on solid substrates (see ref 3,4 for polymeric systems). We do not attempt to provide a detailed, realistic modeling of the surface interactions in the experimental system, but rather utilize a physically reasonable form of these interactions that is able to describe the qualitative features (i.e., first-order wetting of the preferred component) and adjust the strength of the interaction to match the experimental observations.

IV. Binodals and Spinodals in Thin Films

In this section, we analyze the influence of the surface field strength and the film width on the phase behavior. Figure 1 shows typical A and B density profiles for the volume fractions of coexisting phases at $4\Lambda N = 1.4$.

The width of the film is $D_0 = 4.0R_e \approx 133.3$ nm, the regarded Flory−Huggins parameter is $\chi N = 3.7$, which

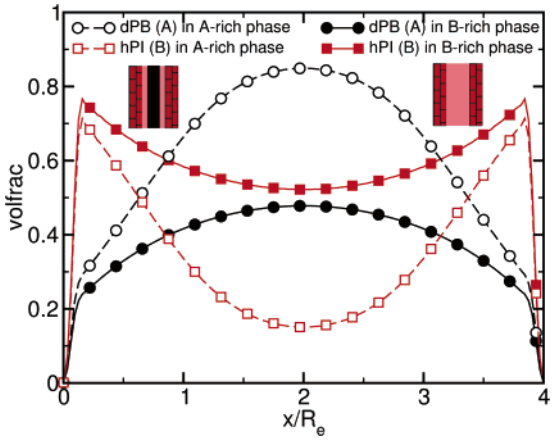

Figure 1. dPB (A) and PI (B) density profiles for the volume fractions at coexistence for $4\Lambda N = 1.4$, film thickness $D_0 = 4R_e \approx 133.3$ nm, and $\chi N = 3.7$ or $T = 62.41$ °C. The surface enrichment of PI at the wall is slightly smaller than in the experiment.[17,18] The A-rich and B-rich phases are sketched on the left- and right-hand side, respectively.

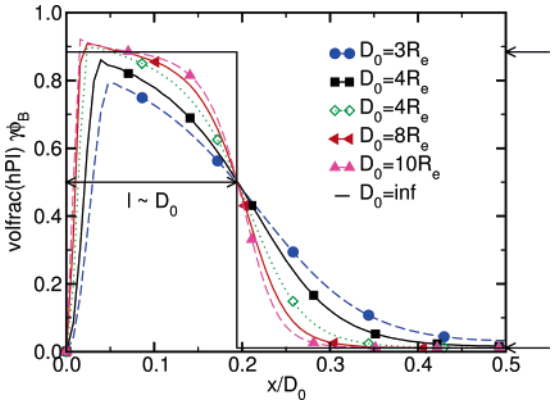

Figure 2. Profiles of the volume fraction of the B-component (PI) for $4\Lambda N = 1.4$, $T = 142.5$ °C ($\chi N = 5.5$), and $\phi = \phi_c = 0.65$. Film thicknesses D_0 are indicated in the key. Arrows on the right mark the volume fractions of the coexisting phases in the bulk.

corresponds to a temperature of $T = 62.41$ °C. ΛN is positive, and therefore, the A component (dPB) is enthalpically attracted to the surfaces. However, the profiles show that the B component (PI) is actually enriched at the surfaces for both volume fractions. This shows that the chosen surface interaction strength does not compensate the entropic preference of the B species to the surface. The profiles of the B-rich phase (closed symbols) show much less spatial variation than the profiles of the A-rich phase (open symbols). In the latter, the B-component is enriched at the surfaces, while A prevails in the center of the film. The two regions are separated by AB interfaces. These internal AB interfaces are not interfaces between thermodynamically coexisting phases (which run perpendicular to the film surfaces), but they resemble the interface between A-rich and B-rich phases in the bulk for large χN or large film thickness.

In Figure 2, we present the composition profile across the film for laterally homogeneous state inside the miscibility gap, $\phi = \phi_c = 0.65$, for various film thicknesses, D_0. Under these conditions, the film will laterally phase separate in equilibrium. The profiles shown in the figure do not correspond to the laterally phase separated, thermodynamic equilibrium but to the laterally homogeneous, metastable state. At a fixed averaged

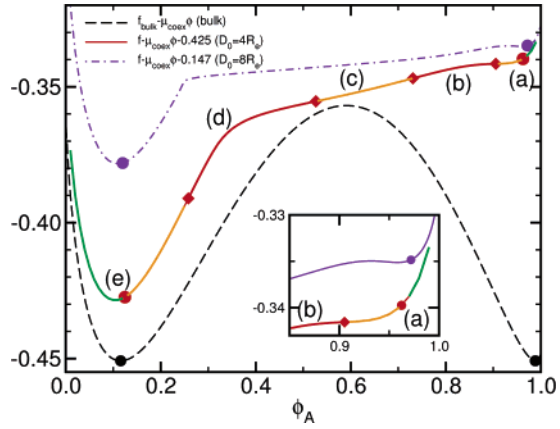

Figure 3. Comparison of the free-energy density of the bulk (cf. eq 19), a thin film ($4\Lambda N = 1.4$ and $D_0/R_e = 4$), and a thicker film ($4\Lambda N = 1.4$ and $D_0/R_e = 8$). Note the extra features on the A-rich side, which mirror the wetting behavior of PI at both surfaces (for an enlarged view see inset). Circles mark the dPB volume fraction at coexistence. Diamonds represent spinodals for $D_0 = 4R_e$. (Meta)stable (a, c, and e) and unstable (b and d) composition regions are indicated.

composition ϕ, there are enrichment layers of thickness $l \sim D_0$, the composition in the enrichment layers is close to the composition of the B-rich phase in the bulk, and the composition in the center of the film is close to the composition of the A-rich phase in the bulk. The internal AB interfaces, which separate the enrichment layers from the center, are weakly bound. The surfaces repel the AB interface as B wets the surface in the semi-infinite system, but the shift of the chemical potential to supersaturation of A limits the growth of the enrichment layers.[30] Upon increasing the film thickness, the interaction between the internal interfaces and the film surfaces becomes weaker, the shift of the chemical potential decreases, such as $\Delta\mu \equiv \mu - \mu_{coex} \sim 1/D_0$ (Kelvin equation), and the internal interfaces resemble the interfaces between A-rich and B-rich phases coexisting in the bulk. It is important to realize that, even for the laterally homogeneous, not phase-separated state, there is no extended region where the composition is close to the average composition. Thus, non bulk-like composition fluctuations around the average composition of the film (i.e., related to the bulk spinodal), but the properties of the internal interfaces (i.e. related to the wetting properties) determine the mode of phase separation.

Within the SCF calculations, one obtains not only the details of the composition profile across the film (as discussed in Figures 1 and 2) but also the free energy associated with such a composition profile. The free energy as a function of the average A composition for the bulk, and for films of width $D_0 = 133.3$ and 266.6 nm, is presented in Figure 3. The regarded temperature is $T = 142.5$ °C or $\chi N = 5.5$. The composition range can be divided into several regions, which we discuss in turn.

(a) Let us start from $\phi_A \to 1$, i.e., a system that is rich in the component dPB that is not preferred by the surfaces. An enlarged view of the composition dependence of the free-energy density, f (see eq 8), is presented in the inset. Starting from an initially pure A-polymer melt, we see that an increase in B reduces the energy of the system. It is favorable for the system to form B enrichment layers near the surfaces. These enrichment layers substitute A at the surface by the preferred

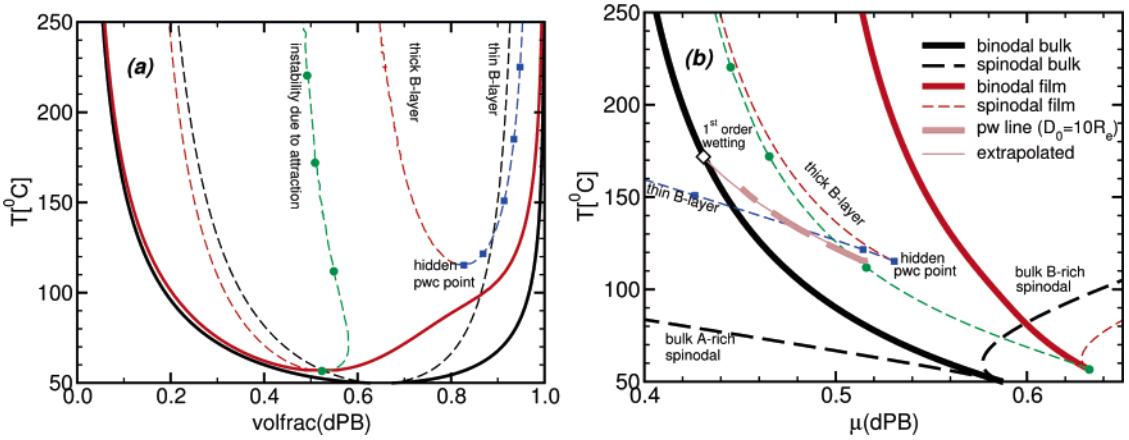

Figure 4. Interplay between spinodal instability and prewetting behavior: Phase diagram in the (**a**) temperature-composition and (**b**) temperature-chemical potential plane for the bulk and a thin film ($4\Lambda N = 1.4$ and $D_0/R_e = 4$). The legend of panel (**b**) also applies for (**a**).

component B and lead to the formation of an internal AB interface at each surface.

(b) After the enrichment layers have been formed, a further increase in B neither changes the composition at the surface nor the densities in the middle of the film. The internal interfaces between A and B are merely shifted toward the middle of the film. The free energy is, hence, dominated by the effective interface potential between the AB interfaces and the confining walls and the interactions between the two interfaces themselves across the film. Regarding the free energy in Figure 3, we observe a shallow barrier between thin ($\phi \sim 0.95$) and thicker ($\phi \sim 0.7$) B enrichment layers. This is the signature of a first-order wetting transition. In our model, we find a first-order wetting transition at around $T \approx 171$ °C for $4\Lambda N = 1.4$. The two inflection points (symbolized by diamonds) between these two regions correspond to the spinodals of a prewetting two-phase region where thin and thick enrichment layers of the B-component coexist. Between the two inflection points, the system is unstable with respect to spinodal dewetting of the enrichment layers. While the prewetting coexistence for this film thickness (see the phase diagram shown in Figure 4) is pre-emptied by lateral phase separation and, thus, does not lead to a two-phase coexistence in a thin film, the prewetting spinodals are still of relevance for the mode of phase separation.[35]

(c) After the thicker enrichment layers have been formed and the enrichment layer is further increased, the two AB interfaces get pushed toward the center of the film, and the free energy becomes rather flat for thick films. The interfaces interact only weakly with the surfaces and only weakly with themselves across the film. For short-range surface fields, the effective interface potential decays exponentially fast with the distance l between the interface and the surface, the length scale is set by the bulk correlation length, ξ_{bulk}. At a fixed composition, the distance l is proportional to the film thickness D_0, and hence, $\ln(df/d\phi) \sim -D_0/\xi_{bulk}$. If the B-component wets the surface, the curvature is positive, i.e., there are very large fluctuations, but the system remains (meta)stable.

(d) As the composition of A decreases further, the interfaces begin to attract each other across the film. This strongly reduces the free energy and eventually leads to the annihilation of the two internal interfaces. Thus, the third spinodal is associated with the instability of the two interfaces against annihilation.

(e) After the annihilation of the two internal interfaces, the composition across the film is fairly uniform, and the behavior on the B-rich side of the phase diagram is similar to the bulk free energy that is given by the Flory−Huggins expression. The spinodal on the B-rich side of the phase diagram is related to the spontaneous growth of bulk-like composition fluctuations analogous to the bulk mixture.

After explaining the general behavior of the free energy as a function of composition, we show the resulting spinodals and binodals of the bulk, and for a film of width $D_0 = 133.33$ nm $= 4R_e$ and $4\Lambda N = 1.4$ in Figure 4**a** as a function of composition and temperature. The merging of the two spinodals far above the wetting transition temperature in the nonwet state occurs at a high temperature, $T > 250$ °C, and is not shown. The two spinodals on the A-rich side of the phase diagram are associated with prewetting behavior. They mark the stability of a thin and a thick enrichment layer of the B-component. Upon decreasing the incompatibility or temperature, the difference between the thin and the thick enrichment layer decreases, and the two spinodals join at the hidden, prewetting critical point (pwc). Another indication that the spinodals on the A-rich side are due to prewetting comes from the corresponding phase diagram in the $T-\mu$ plane. In Figure 4**b**, we have drawn the coexistence curves and spinodals in the bulk, and the prewetting line (as extracted from a film of width $D_0 = 10R_e$). The latter emerges from the bulk coexistence curve at the wetting transition temperature (marked by an empty diamond) and continues into the supersaturated region of A. It ends at the prewetting critical point. The coexistence curve of a film is shifted away from the bulk coexistence curve into the supersaturated region of A. The shift in chemical potential is inversely proportional to the film thickness (Kelvin equation). For the rather thin film considered, the shift is large and the prewetting line does not cross the coexistence curve of the film. Therefore, the prewetting behavior does not influence the binodals much. The two spinodals that are located on the A-rich side of the phase diagram are just slightly shifted away from the prewetting spinodals of the semi-infinite system (not shown) in the $T-\mu$ plane. The two spinodals that are located on the B-rich side of the phase diagram join at the critical point of the thin film. They resemble the spinodals in the bulk in the temperature−chemical

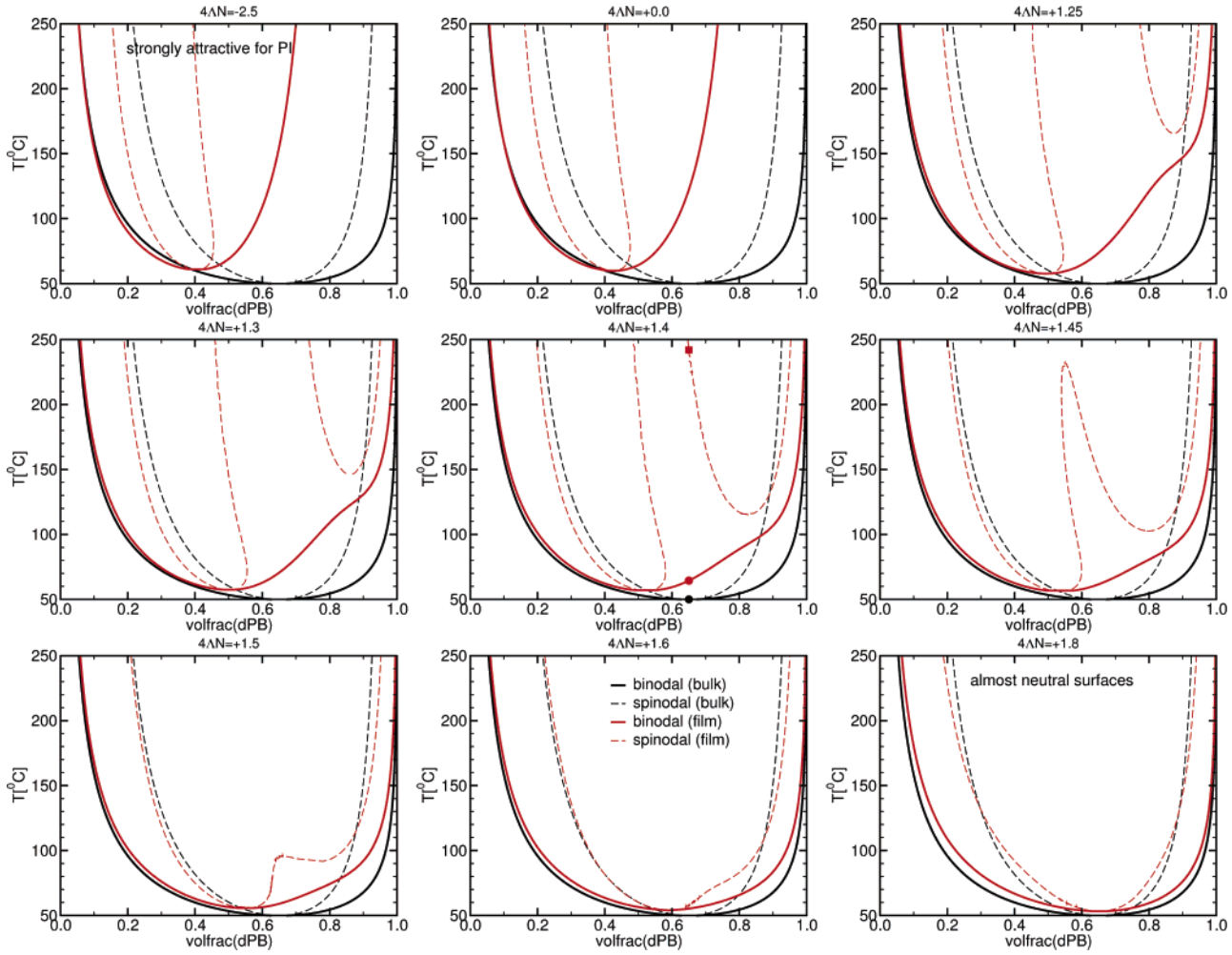

Figure 5. Dependence of binodals and spinodals on the strength of the surface fields ΛN at film thickness $D_0/R_e = 4$. Solid lines represent the binodals in the bulk and the thin film, while dashed lines present spinodals.

potential plane, but are slightly shifted to larger μ (Kelvin equation).

The dependence of binodals and spinodals on the strength of the surface fields is illustrated in Figure 5. The surfaces are symmetrical, and from the top left to the bottom right panel, we successively increase $4\Lambda N$ from -2.5, when the walls strongly attract PI, to $+1.8$, when the walls are almost neutral.

For the strongest surface field, there is a large shift in the critical point both to smaller volume fraction of A and higher temperature. As the surface interactions are strong, PI wets the surface at all temperatures considered, and even the prewetting critical point is at high temperature $T > 250$ °C. Therefore, only the two spinodals associated with the attraction of the two AB interfaces and the B-rich bulk are visible.

As we decrease the surface attraction, the wetting transition shifts to lower incompatibility, and for $4\Lambda N = 1.25$, the hidden prewetting critical point shifts into the temperature range considered. The prewetting behavior gives rise to a "bulge" in the A-rich binodals.[20] As we make the surfaces less attractive for B, the merging of the two spinodals (instability against attraction of the two interfaces and instability of thick B-enrichment layers at surfaces) also becomes observable at around $T \approx 232$ °C for $4\Lambda N = 1.45$. Approaching neutral surface fields, we observe that the wetting transition approaches the critical point, the prewetting line becomes shorter (i.e., the wetting transition becomes weaker), and its influence on the binodals, the "bulge", and spinodals, the merging temperature of the two spinodals, gradually vanishes. For neutral surfaces, there is no wetting transition, the critical point is shifted to slightly higher incompatibility than in the bulk, and the spinodals in a film resemble the bulk spinodals. Note that there is a gradual change from the behavior of neutral surfaces to the behavior of surfaces which strongly prefer the B-component. The behavior of the spinodals for strong and moderate surface fields, however, differs qualitatively from the behavior of the binodals for neutral surfaces and in the bulk. Specifically, there is a "channel of metastability" around $\phi = \phi_c = 0.65$, which extends to rather high temperatures.

So far, we have only regarded one film width and studied the change in surface interaction strength. We now study the influence of varying film thicknesses at the fixed surface field strength $4\Lambda N = 1.4$. The binodals and spinodals for film thicknesses $D_0 = 3$, 4, 8, and $10R_e$ are presented in Figure 6.

For very small film widths ($D_0 = 3R_e \approx 100$ nm), D_0 is not much larger than the width of the AB interface at the prewetting critical temperature. As a consequence, there is no temperature at which the interaction (attraction) between the two interfaces can be neglected, and the prewetting behavior that is associated with a single surface is strongly distorted. Hence, the two spinodals associated with the attraction of the two

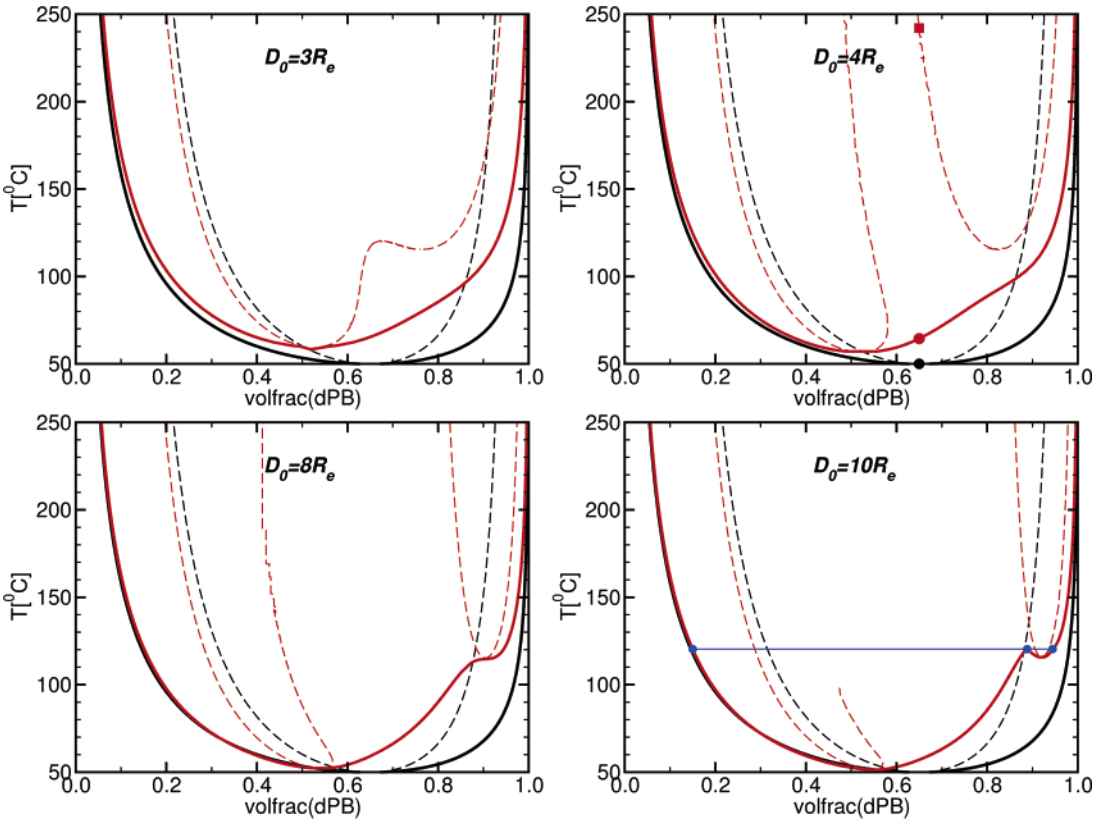

Figure 6. Dependence of binodals and spinodals on the film thickness $D_0/R_e = 3$, 4, 8, and $10R_e$ at $4\Lambda N = 1.4$. Solid lines represent the binodal in the bulk and the thin film, while dashed lines present spinodals. Only part of the spinodal attributable to the attraction of the two internal interfaces is shown in the bottom right panel ($D_0 = 10R_e$) because the free energy in this region hardly varies with composition, and it becomes numerically difficult to locate the spinodal.

interfaces and the instability of thick B-layers at the surfaces merge already at rather low incompatibility. Upon increasing the film thickness, the enrichment layers at the two surfaces are further apart, or in other words, the interfaces interact less, and the prewetting behavior of the spinodals is observed much more clearly. Because the prewetting-like spinodals are associated with enrichment layers of finite thickness, both the distance between the two branches of the spinodal and the distance from $\phi = \phi^{bulk}_{Acoex}$ scales, such as $1/D_0$ in the composition, i.e., the prewetting spinodal region becomes narrower and gets squeezed to the right side of the phase diagram with increasing film width. For large film thickness $D_0 > 8R_e$, the prewetting line crosses the coexistence curve in a film, and a triple point between a B-rich phase and A-rich phases with thin and thick enrichment layers of B at the surfaces, forms.[20,31,32] Below the triple point, the prewetting coexistence gives rise to a two-phase region, which ends in the prewetting critical point. This is illustrated in the bottom right panel. Only part of the spinodal associated with the interaction between the two formed AB interfaces is shown because the flatness of the free-energy density, cf. Figure 3, makes the determination of its location numerically difficult. The study of the film thickness dependence shows that, even in the limit of large film widths, the spinodals of a thin film do not gradually approach the spinodals of the bulk. The binodals of a film with symmetric surface interactions do approach the bulk behavior; the second two-phase region attributable to prewetting becomes a thin line in the limit $D_0 \rightarrow \infty$.

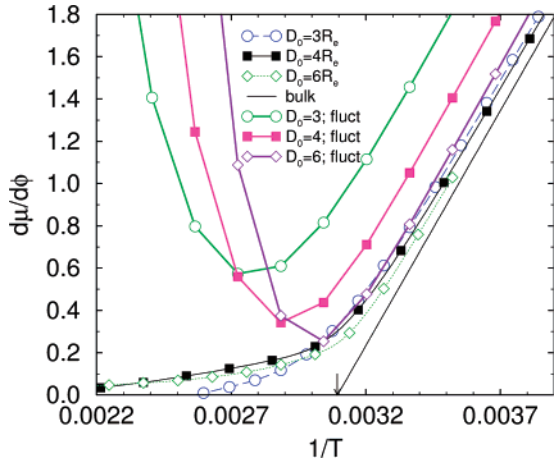

Figure 7. Inverse scattering function as a function of inverse temperature at the bulk critical composition $\phi^{bulk}_{A,c} = 0.65$ and $4\Lambda N = 1.4$ for film thicknesses $D_0/R_e = 3$, 4, 6. Thin lines describe the actual susceptibility, $(d\mu/d\phi)|_{film}$, obtained from one-dimensional SCF calculations. Thick lines are the results from the "simulated" perpendicular scattering. The arrow marks the inverse bulk critical temperature.

V. Scattering in Thin Films

In this section, we study scattering by analyzing the energy cost of exciting different composition modes instead of performing the tedious calculation of the scattering factor. Although this will not give quantitative results, the comparison with the experiments should give a qualitative estimate.

Figure 7 shows the derivative $(d^2f/d\phi^2) = (d\mu/d\phi)$ at the bulk critical composition $\phi_c = 0.65$ as a function of

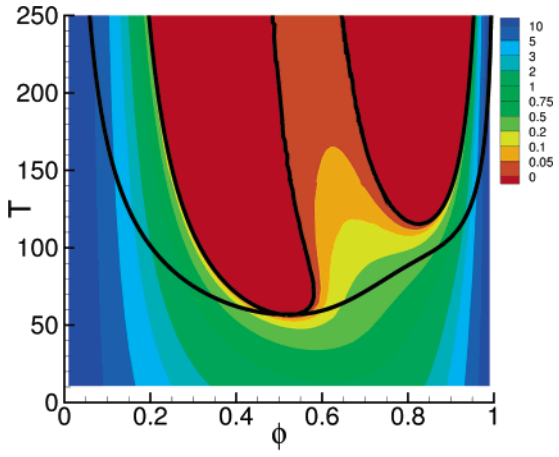

Figure 8. Contour plot of $(d\mu/d\phi)|_{film}$ for film thickness $D_0 = 4R_e \approx 133.3$ nm and $4\Lambda N = 1.4$. Solid lines mark binodals and spinodals.

inverse temperature. The results denoted by thin lines were obtained by taking the second derivative of $f(\phi)$ obtained from the SCF calculations with respect to the change in average composition of the system. This change of the average composition across the film corresponds to a composition wave with a vanishing component of the wave vector parallel to the film $q_{||} \rightarrow 0$ (cf. also below).

An illustration of the inverse susceptibility $(d\mu/d\phi)$ as a function of both temperature and composition is presented in Figure 8 for a film of width $D_0 = 4R_e \approx 133.3$ nm, and the surface interaction strength $4\Lambda N = 1.4$. For these parameters, there is a narrow "channel of metastability" around the critical composition, where the susceptibility is very large but finite.

In the one-phase region, $\chi < \chi_c$ or $1/T > 1/T_c$, we find a linear dependence of the inverse susceptibility on the inverse temperature or Flory–Huggins parameter. The slope of the linear behavior is comparable with the slope in the bulk, indicating that fluctuations chiefly stem from bulk-like composition fluctuations. In agreement with the common procedure of analyzing scattering data in the bulk, one can extrapolate this linear behavior of the inverse scattering intensity in the one-phase region to estimate the location of the spinodal according to

$$\frac{d\mu}{d\phi} \sim \frac{1}{S_{coll}(q \rightarrow 0)} \sim \chi - \chi_s(\phi) \qquad (25)$$

the result of the random-phase approximation for the bulk. S_{coll} denotes the structure factor of composition fluctuations and $\chi_s(\phi)$ the value of the Flory–Huggins parameter at the (mean field) spinodal ("extrapolated spinodal").

At larger incompatibility, $\chi > \chi_c$, enrichment layers form, and the susceptibility is determined by fluctuations of the internal interfaces rather than by bulk composition fluctuations. In marked contrast to the bulk, the susceptibility arises from qualitatively different effects in the one- and two-phase region. This is clearly visible in the change in slope of the inverse scattering intensity. This change in the slope in our calculations thus indicates the formation of enrichment layers at the surfaces and the change of the character of fluctuations from homogeneous, bulk-like to capillary wave-like fluctuations in the local position of the internal dPB/PI interfaces that separate the PI enrichment layers from the dPB-rich center of the film.[36]

Extrapolating experimental results from the one-phase region into the miscibility gap yields at best qualitative estimates. This holds particularly true in the "channel of metastability", where the spinodal is deeply buried in the miscibility gap and one has to extrapolate a long way. From the behavior in the vicinity of the bulk critical temperature, the location of the spinodal in the film can only be estimated qualitatively.

If we were to extrapolate the linear regime of $(d\mu/d\phi)$ (or our estimate for the inverse perpendicular scattering intensity, cf. below) at large values of $1/T$ to $(d\mu/d\phi) = 0$, we observe that the resulting "extrapolated spinodal" temperatures are somewhat larger than the bulk spinodal/critical temperature. In agreement with the experiment,[15] such an extrapolation from the one-phase region suggests that the spinodal temperature T_s, and thus, the shift from the bulk spinodal would decrease as one increased the film thickness, D_0. This result of the extrapolation (obtained from both, experiments and SCF calculations) is in contrast to the behavior of the true thermodynamical spinodal. The latter shifts to higher temperatures, i.e., further away from the bulk spinodal, as we increase the film thickness.

To "simulate" scattering perpendicular to the film, we excite the equilibrium profile perpendicular to the film with the antisymmetric composition mode with the smallest wave vector $q_{\perp,min} = 2\pi/D_0$ allowed by the finite film thickness. To this end, we fix the amplitude of the composition mode with $q_{\perp,min}$ and minimize the free energy of the constrained system within SCF theory. Because the profile is no longer symmetrical across the midplane of the film, composition modes with even indices, $i = 4, 6, \ldots$ in eq 17, also need to be taken into account. The difference in free energy between the constrained system and the system with symmetric equilibrium profiles depends quadratically on the amplitude, $\varphi_{q\perp,min}$, of the excitation, and $\partial^2 f/\partial\varphi^2_{q\perp,min}$ provides us with a qualitative estimate for the inverse structure factor, $S^{-1}(q_{\perp,min})$, perpendicular to the wall.

The so-determined estimate, $S^{-1}(q_{\perp,min})$, as a function of inverse temperature for different film thicknesses, is displayed in Figure 7 through the thick lines. For larger values of $1/T$ (one-phase region), the behavior is qualitatively similar to the inverse susceptibility $(d\mu/d\phi)$. A linear behavior of the inverse structure factor is observed with a slope that is comparable to the bulk. In this region, we find that the smaller the film width the more pronounced the shift away from the bulk values. The performed excitation leads to an additional density gradient perpendicular to the film. Using the squared gradient expansion, the first approximation of the energy shift through the excitation $\delta\phi(x)$ can be seen as

$$\Delta F \approx \frac{1}{2}\int dx \left(\frac{d^2 f_{bulk}}{d\phi^2} + a\Delta_\perp\right)(\delta\phi(x))^2 \qquad (26)$$

with a being almost constant. Hence, the shift away from the inverse bulk susceptibility should be proportional to $\Delta_\perp \sim q^2_{\perp,min} \sim 1/D_0^2$. This expected behavior is clearly shown through the line in Figure 9, where we have plotted the shift away from the bulk as a function of $1/D_0^2$ both for the actual susceptibility, $(d\mu/d\phi)|_{film}$ obtained from SCF calculations (circles) and for the antisymmetric excitation (squares).

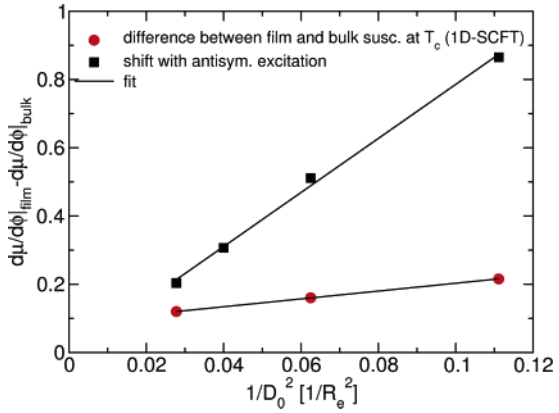

Figure 9. For small temperatures (in the one-phase region), the calculated scattering functions show a comparable linear behavior as in the bulk. Here, the shift away from the bulk line is plotted as a function of $(1/D_0)^2$.

If we go to higher temperatures, in Figure 7, we find that the inverse scattering function strongly increases. Why this occurs can be explained through Figure 10, which shows the second derivative of the bulk free energy with respect to the composition for different temperatures as a function of the composition $\gamma\phi_B$ in the top left panel (**a**) and the equilibrium profiles $\gamma\phi_B(x)$ of a film of width $D_0 = 3R_e$ for the respective temperatures in panel (**b**). The top right panel (**c**) shows $(d\mu/d\phi)$ as a function of the distance from the walls, which is obtained by inserting the density profiles $\phi(x)$ for different temperatures in eq 21 for the inverse bulk susceptibility. The squared sine function $(\delta\phi(x))^2$ in (**b**) and (**c**), of which the amplitude in the graph has been strongly exaggerated compared to the largest used for the calculations, makes clear where in the film the density is influenced by exciting the lowest antisymmetric density mode. The density is not changed at the walls and in the middle of the film. The main change takes place in the region near the interfaces. If we look at the lower values of T, the densities in the regions, where the excitation has the most influence, are in the interval $0.3 < \phi < 0.5$. If we look at the top left panel, we see that $d^2f/d\phi^2$ for a constant temperature is almost constant and small in this density interval. In panel (**c**), we see accordingly that the inverse susceptibility is nearly constant across the whole film. For intermediate values of $T < 70$ °C, the inverse susceptibility across the film stays almost homogeneous but decreases to lower values with increasing temperature. The free energy necessary for scattering decreases, and therefore, the inverse structure factor also decreases. Upon increasing the temperature further, the density profiles show enrichment layers with higher densities and sharper interfaces. Regarding the left and the top right panels, we see that in the regions of the interfaces the excitation is energetically favorable for the system. The sine function, however, also leads to a change in density in regions where the densities are very far from the bulk critical density. If we look at $T = 172$ °C, for example, regions where the densities are about $\gamma\phi_B = 0.75$ and $\gamma\phi_B = 0.05$ are influenced by the excitation. The top right panel shows that a change in density in these regions is very expensive. Although the density is mainly influenced near the interfaces, the slight change in density near the walls and the middle of the film costs so much energy that the inverse structure factor increases with higher temperatures as observed in Figure 7.

We expect scattering parallel to the film to lead to qualitatively similar results. But by scattering, in other words by exciting density modes parallel to the film, the density profiles perpendicular to the films will be changed in a different way. Instead of profiles acquiring an antisymmetric component, they should remain symmetric. It can be seen as a fluctuation parallel to the walls of the average density; the profiles across the film should be comparable with equilibrium profiles simply at higher or lower compositions of B-polymers. In this case, it is important to bear in mind that the change in profiles changes density modes with wave vectors that

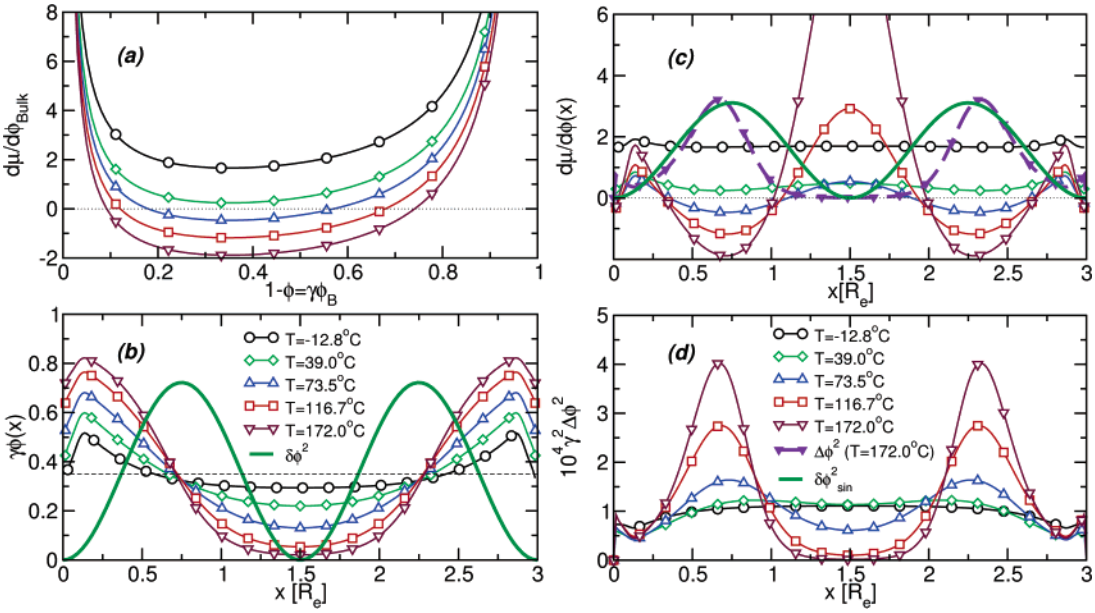

Figure 10. (**a**) $d^2f^{bulk}/d\phi^2$ in the bulk (cf. eq 21) as a function of the average composition $\gamma\phi_B$ for different temperatures. (**b**) Equilibrium density profiles in a film of thickness $D_0 = 3R_e$ and an average composition of $\bar{\phi}_A = 0.65$ for the respective temperatures of panel (**a**). The sine function indicates where the density is influenced most by exciting the first antisymmetric density mode. (**c**) $(d\mu/d\phi)$ as a function of the distance x from the walls. (**d**) Squared density changes $\gamma^2(\Delta\phi(x))^2$ as a function of position x perpendicular to the film for different temperatures.

have components perpendicular to the film. To get a complete picture of this parallel scattering, it would be necessary to calculate the explicit inverse structure factor.

To get a rough insight into this kind of scattering, i.e., to find out which regions will mainly contribute to scattering, we have looked at the differences in the equilibrium profiles between the average composition at $\gamma\bar{\phi}_B = 0.65$ and $\gamma\bar{\phi}_B = 0.64$. In Figure 10**c**, the inverse susceptibility as a function of the equilibrium density profile and the squared density change for the perpendicular sine excitation (no symbols) and for the shift in average composition $(\Delta\phi_B(x))^2 = (\phi_{B,\bar{\phi}=0.65}(x) - \phi_{B,\bar{\phi}=0.64}(x))^2$ for $T = 172$ °C are shown (closed symbols). The bottom panel (**d**) displays the squared density differences $(\Delta\phi_B(x))^2$ at different temperatures. All results are for a film of thickness $D_0 = 3R_e$. For lower temperatures, we see that the change in density is almost uniform across the whole of the film. The inverse susceptibility is also very uniform but decreases with higher temperatures. The whole film will contribute to the scattering, but the inverse structure factor will decrease in a similar fashion as for the antisymmetric excitation. This uniform change in the density is equivalent to adding a constant, i.e., a $q_\perp = 0$ mode to the density profile. Therefore, the squared gradient term in the free energy, see eq 26, will lead to a negligible contribution so that the shift of the scattering function away from the bulk susceptibility will not be as pronounced as was the case for the antisymmetric excitation, see Figures 7 and 9.

With increasing temperature, the change in the middle of the film stays almost the same, but near the walls, the change decreases, which follows from the saturation of the densities at the walls. With increasing temperature, the slope of the interfaces becomes steeper and the enrichment layer widens, therefore, the density difference is mainly visible in the region of the formed interface. For higher temperatures, the change in average density is hardly visible in the middle of the film; the only change that takes place is the shift of the interface. If we look at the susceptibility in the region of the interface, we find that it is negative, and therefore, the system would gain energy. The system is obviously unstable and phase separation would occur. Contrary to results obtained through the antisymmetric excitation where the inverse scattering function rose with higher temperatures because of the change in density near the edges of the interface, the density change caused through parallel "scattering" is localized near the interface, leading to a much larger response.

VI. Conclusions

In this paper, we performed SCF calculations for a dPB/PI blend at bulk critical composition confined between two hard symmetric walls. The calculations were performed to give an insight into the equilibrium phase behavior of such systems. In this paper, we focus on the phase diagrams, including both spinodals and binodals as a function of film width and wall−polymer interaction strength. We further analyzed the effects of scattering in polymer films. The study of spinodals reveals that the behavior is clearly different from the behavior in the bulk. While spinodals and binodals are comparable in the bulk, they can differ considerably in a thin film. Instabilities in the bulk are caused by composition fluctuations; in a thin film, however, fluctuations of formed interfaces are mainly responsible for causing phase separation. Instead of finding the usual spinodal, we find two sets of spinodals in thin films that are caused by the intricate interplay of prewetting and spinodal instability. The two spinodals on the dPB-rich side mark the instability between thick and thin enrichment layers near the walls, while the spinodal on the PI-rich side is caused by the interaction between the two formed dPB/PI interfaces, and only the spinodal close to the dPB-poor binodal corresponds to the spinodal in the bulk. The examination of increasing film widths further shows that the thin film behavior does not gradually approach the bulk behavior, but there remains a "channel of metastability" where the film at bulk critical composition remains metastable deep into the miscibility gap.

To study scattering perpendicular and parallel to the film, we regarded conformations with certain excited density modes. Similar to the typical experimental practice, we analyzed the inverse structure factor as a function of inverse temperature. For small temperatures, the slope of the actual inverse susceptibility obtained from SCF calculations and the simulated scattering is comparable to that of the bulk. With increasing temperature, the inverse susceptibility bends away from the bulk behavior, leading to a spinodal temperature that is much larger than in the bulk. When scattering perpendicularly to the film, we find that the inverse structure factor has a minimum and increases again for increasing temperature. This can be explained because scattering leads to changes in density in regions of the film where these are energetically very expensive. For parallel scattering in the regarded films, we argue that the theoretical inverse structure factor should become negative with increasing temperature, or in other words, phase separation would occur spontaneously.

To determine the spinodal temperature experimentally, the inverse structure factor is commonly extrapolated to zero.[15] Our theoretical study shows that this kind of an extrapolation also leads to a shift of the temperature in the right direction. The behavior of the inverse susceptibility, though, shows that this extrapolation is only capable of giving a qualitative estimate. A quantitative conclusion cannot be drawn. Although this method is useful for bulk experiments, it is not appropriate for quantitatively determining the spinodal temperature in a thin polymer film.

Our calculations have been restricted to strictly equilibrium situations and focused on the equilibrium thermodynamic behavior, paying particular attention to the influence of the wetting behavior on fluctuations in thin films. These are rather universal features that only depend on qualitative properties of the system (like the fact that the system exhibits a first-order wetting transition).

We did not attempt to compare our predictions of the composition profiles across the film with experimental results.[17,18] Unlike the rather universal behavior of the spinodals, profiles do depend on the details of the surface interactions that comprise long-range van der Waals contributions, short-range contributions due to the distortion of the composition profile in the vicinity of the surface, as well as local entropic and enthalpic effects on the length scale of a few statistical segments. Some of these effects might counteract each other (e.g., even in our simple model entropic packing effects and short-range, enthalpic surface interactions favor differ-

ent components at the surface) and give rise to rather intricate behavior.

Within the SCF theory, the composition profile, $\phi_A(x)$, is a functional of the surface interaction, $H(x)$, and in principle, one might hope to estimate the detailed form of the surface interaction by matching the profiles calculated by the SCF theory with the experimentally measured profiles and thus learn about the nature of the surface interactions. Unfortunately, this procedure is difficult in practice for the following reasons: (i) The matching between experimental profiles and SCF predictions only provides an estimate of the effective free energy of the polymer−surface interactions. It is difficult to separate this quantity into enthalpic effects, like van der Waals interactions and short-range contact interactions, and entropic contributions, like those described by eq 24 and additional contributions that may arise from liquid-like packing effects on the scale of a statistical segment, which would have to be described by a nonlocal free-energy functional. Thus, for instance, the surface free-energy field, $H(x)$, that matches the experimentally observed profile depends on the specific choice of the total density profile, $\Phi_0(x)$. (ii) Capillary waves lead to a broadening of the interface profiles. These fluctuations of the local interface position are not captured by the SCF theory, and this approximation leads to an erroneous identification of the surface interactions. For thin enrichment layers, however, the AB interface interacts strongly with the surface, and the strong interface potential imparts a small lateral correlation length onto the capillary waves of the bound interface, which results, in turn, in a strong reduction of capillary wave broadening.[33] (iii) Moreover, the error in the experimental data translates into a rather significant uncertainty in the effective free energy of the polymer−surface interactions. Thus, a major challenge remains to extract the detailed form of the surface interactions from experimental observations.

An additional reason for deviations between SCF calculations and experiments might be nonequilibrium effects attributable to the strong attraction of one species to the film surfaces that might lead to irreversible adsorption. For instance, the shape of density profiles obtained by Grüll et al.[17,18] for thin dPB/PI films appears not to be explicable within a squared gradient approach,[34] suggesting that an immobile "gel" layer is formed at the surfaces. These effects are outside the realm of the present work.

Acknowledgment. Financial support by the DFG (Mu1674/1 and 3) as well as the NSF (DMR-0113756) are gratefully acknowledged. Computing time has been provided by the NIC Jülich and the HLR Stuttgart.

References and Notes

(1) Budkowski, A. *Adv. Polym. Sci* **1999**, *148,* 1.
(2) Geoghegan, M.; Krausch, G. *Prog. Polym. Sci.* **2003**, *28,* 261.
(3) Rysz, J.; Budkowski, A.; Bernasik, A.; Klein, J.; Kowalski, K.; Jedlinski, K.; Fetters, L. J. *Europhys. Lett.* **2000**, *50*, 35.
(4) Geoghegan, M.; Ermer, H.; Jüngst, H.; Krausch, G.; Brenn, R. *Phys. Rev. E* **2000**, *62*, 940.
(5) Binder, K. *Adv. Polym. Sci.* **1999**, *138,* 1.
(6) Müller, M.; Albano, E. V.; Binder, K. *Phys. Rev. E* **2000**, *62,* 5281.
(7) Edwards, S. F. *Proc. Phys. Soc.* **1965**, *85,* 613.
(8) Helfand, E. *J. Chem. Phys.* **1975**, *62,* 999.
(9) Fredrickson, G.; Ganesan, V.; Drolet, F. *Macromolecules* **2002**, *35,* 16.
(10) Müller, M.; Schmid, F. *Adv. Polym. Sci* **2005**. In press.
(11) Müller, M. In *Soft Condensed Matter*; Gompper, G., Schick, M., Eds.; John Wiley & Sons: New York, 2005.
(12) Binder, K. *Phys. Rev. A* **1984**, *29,* 341.
(13) Wang, Z.-G. *J. Chem. Phys.* **2002**, *117,* 481.
(14) Balasra, N. P.; Rappl, T. J.; Lefebvre, A. A. *J. Polym. Sci., Part B* **2004**, *42,* 1793.
(15) Jones, R. L.; Indrakanti, A.; Briber, R. M.; Müller, M.; Kumar, S. K. *Macromolecules* **2004**, *37,* 6676.
(16) Akpalu, Y. A.; Karim, A.; Satija, S. K.; Balsara, N. P. *Macromolecules* **2001**, *34,* 1720.
(17) Grüll, H.; Schreyer, A.; Berk, N. F.; Majkrzak, C. F.; Han, C. C. *Europhys. Lett.* **2000**, *50,* 107.
(18) Grüll, H.; Sung, L.; Karim, A.; Douglas, J. F.; Satija, S. K.; Hayashi, M.; Jinnai, H.; Hashimoto, T.; Han, C. C. *Europhys. Lett.* **2004**, *65,* 671.
(19) Flebbe, T.; Dünweg, B.; Binder, K. *J. Phys. II* **1996**, *6,* 667.
(20) Müller, M.; Binder, K. *Macromolecules* **1998**, *31,* 8323.
(21) Reister, E.; Müller, M. *J. Chem. Phys.* **2003**, *118,* 8476.
(22) Müller, M.; Binder, K. *J. Phys.: Condens. Matter* **2005**, *17,* 333.
(23) Vavasour, J. D.; Whitmore, M. D. *Macromolecules* **1993**, *26,* 7070.
(24) Matsen, M. W. *J. Chem. Phys.* **1997**, *106,* 7781.
(25) Geisinger, T.; Müller, M.; Binder, K. *J. Chem. Phys.* **1999**, *111,* 5241.
(26) Doi, M.; Edwards, S. F. *The Theory of Polymer Dynamics;* Oxford University Press: New York, 1994.
(27) Dennis J. Jr.; Schnabel, R. *Numerical Methods for Unconstrained Optimization and Nonlinear Equations;* Prentice-Hall: Englewood Cliffs, NJ, 1983.
(28) Lifshitz, I. M.; Grosberg, A. Yu.; Khohklov, A. R. *Rev. Mod. Phys.* **1978**, *50,* 683.
(29) Schick, M. In *Liquids at Interfaces,* Les Houches, Session XLVIII, Charvolin, J., Joanny, J. F., Zinn-Justin, J., Eds.; Elsevier: Amsterdam, 1990.
(30) For a thin film with short-range surface forces, this balance leads to a logarithmic increase of the thickness l of the enrichment layers with film thickness D_0 at coexistence. See, e.g., Parry, A. O.; Evans, R. *J. Phys. A* **1992**, *25,* 275.
(31) Evans, R.; Marconi, U. M. B. *Phys. Rev. A* **1985**, *32,* 3817.
(32) Nicolaides, D.; Evans, R. *Phys. Rev. B* **1989**, *39,* 9336.
(33) Werner, A.; Schmid, F.; Müller, M.; Binder, K. *J. Chem. Phys.* **1997**, *107,* 8175.
(34) Indrakanti, A.; Jones, R. L.; Kumar, S. K. *Macromolecules* **2004**, *37,* 9.
(35) Here, we have described the typical situation that the B-component wets the surfaces. Far above the wetting transition, $\chi N \gg \chi N_{wet}$, in the nonwet state, the surfaces strongly attract the AB interfaces. There is no prewetting coexistence, and hence, there is no such region (b). In this case, there are only two spinodals located close to the binodals of the film.
(36) This change of slope in Figure 7 should not be confused with the change of slope observed in experiments. In the latter case, it signals phase separation, i.e., the transition from a laterally homogeneous sample to the formation of laterally coexisting domains. Thus, one can extract from the change of slope of the experimental data the location of the binodal.[15]

MA0473465